Data Consistency Conditions for Cone-Beam Projections on a Circular Trajectory

Rolf Clackdoyle, Laurent Desbat, Jérôme Lesaint, and Simon Rit

***Abstract*—The well-known Helgason–Ludwig data consistency conditions (DCCs) for parallel projections of a two-dimensional function take the form of homogeneous polynomials in $\cos\phi$ and $\sin\phi$, where ϕ is the angle of the parallel projection. In this note, we establish necessary DCCs for cone-beam (CB) projections of a three-dimensional function taken along a circular trajectory. Our DCCs take the form of homogeneous polynomials in $\cos\lambda$ and $\sin\lambda$, where λ is the angular position of the CB projection. This trigonometric polynomial format for the DCCs is particularly convenient for medical imaging applications, and these new DCCs for the standard CB geometry will potentially lead to new DCC applications in X-ray computed tomography (CT) and pinhole single photon emission computed tomography (SPECT) where CB projections are measured. If, as is usually the case, the object intersects the trajectory plane, then singularities appear in the DCC formulas. We describe how to interpret and handle these singularities as generalized functions. Numerical simulations are provided for illustration.**

I. Introduction

IN IMAGE reconstruction from projections, data consistency conditions (DCCs) are mathematical expressions that precisely describe the small redundancy that exists between projections. For the case of parallel projections, complete (necessary and sufficient) DCCs have been known for some time [1], [2]. They are known as the Helgason–Ludwig conditions and they take the form of trigonometric polynomials. DCCs are also known for parallel projections that have undergone constant exponential attenuation [3], and in the 2-D case, spatially-varying attenuation [4]. These DCCs have seen extensive applications in positron emission tomography (PET) [5]–[9], and in single photon emission computed tomography (SPECT) [10]–[13].

For applications in X-ray computed tomography (CT), the projections are collected in fan-beam or cone-beam (CB) format. There has been a number of descriptions of DCCs for fan-beam [14]–[23] and for cone-beam [14], [15], [18], [24]–[29] geometries. However, satisfactory DCCs for divergent projections have yet to be established for the common situation of a circular trajectory of the X-ray source, with the detector positioned opposite and moving in tandem with the source. For these cases of circular source trajectories, there are still no conditions known where a small finite collection of cone-beam or fan-beam projections can be evaluated directly for consistency. Some of the conditions require *all* projections, uniformly sampled on the whole circle (or at least on a short scan) so that a simple conversion to parallel geometry is possible. Several of the published conditions do allow a pairwise consistency evaluation of divergent projections, but implementation of this method tends to be cumbersome. However, one recent method [29] forms a weighted sum of the CB projections whose DCC is independent of the projection angle, similar to the order-zero Helgason–Ludwig conditions. The work we present here is a generalization of this result to higher orders.

In Section II, we first review the Helgason–Ludwig conditions, in particular to note the trigonometric form. We then introduce and prove CB DCCs that are of the same convenient trigonometric form. Section III concerns illustrations using computer simulations.

Manuscript received August 11, 2016; revised September 28, 2016; accepted September 29, 2016. Date of publication October 7, 2016; date of current version October 31, 2016. This work was supported in part by Grant ANR-12-BS01-0018 (project "DROITE") from the Agence Nationale de la Recherche. The associate editor coordinating the review of this manuscript and approving it for publication was Prof. Edmund Y. Lam.

R. Clackdoyle, L. Desbat, and J. Lesaint are with the TIMC-IMAG laboratory (CNRS UMR 5525), Université Grenoble Alpes, 38000 Grenoble, France (e-mail: rolf.clackdoyle@univ-grenoble-alpes.fr; laurent.desbat@imag.fr; lesaint.jerome@gmail.com).

S. Rit is with the CREATIS laboratory (CNRS UMR 5220), INSA Lyon, 69621 Villeurbanne, France (e-mail: simon.rit@creatis.insa-lyon.fr).

Digital Object Identifier 10.1109/LSP.2016.2616026

II. Data Consistency Conditions

A. Helgason–Ludwig Conditions

We briefly review the Helgason–Ludwig conditions. In two dimensions, we define the conventional parallel projection $p(\phi,\cdot)$ at angle ϕ of the density function f by

$$p(\phi,r)=\mathcal{R}f(\phi,r)=\int_{-\infty}^{\infty} f(r\alpha_\phi+s\beta_\phi)\,ds \tag{1}$$

for $\phi\in[0,\pi)$, $r\in(-\infty,\infty)$, where $\alpha_\phi=(\cos\phi,\sin\phi)$ and $\beta_\phi=(-\sin\phi,\cos\phi)$.

For each nonnegative integer n, the nth moment of the projection is defined by

$$J_n(\phi)=\int_{-\infty}^{\infty} p(\phi,r)\,r^n\,dr. \tag{2}$$

Now if $p=\mathcal{R}f$ for some f, then $J_n(\phi)$ will be a homogeneous polynomial of degree n in $\cos\phi$ and $\sin\phi$, i.e.,

$$J_n(\phi)=\sum_{k=0}^{n} A_k\ \cos^{n-k}\phi\ \sin^k\phi. \tag{3}$$

Equations (2) and (3) are called the nth-order Helgason–Ludwig conditions and they follow easily from (1). We do not discuss the converse here.

These conditions are particularly useful for applications because they are in "projection form" (see [20]) and allow a finite number of arbitrarily oriented projections to be checked for consistency. On the other hand, if all projections are available

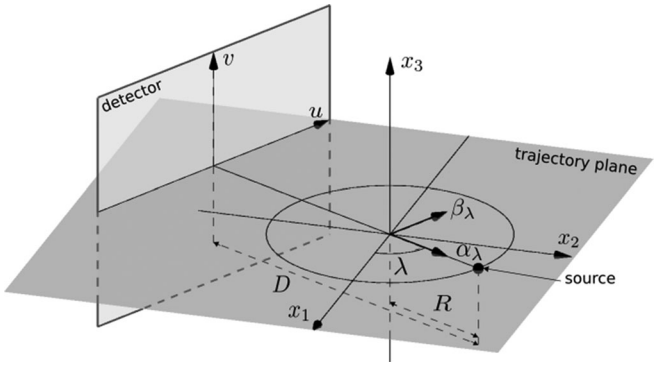

Fig. 1. The CB geometry. The source travels along a circular trajectory of radius R in the $x_3 = 0$ plane. The detector is distance D from the source, oriented conventionally. The perpendicular unit vectors α_λ and β_λ respectively indicate the direction of the source and the u-direction on the detector. The v-direction is parallel to the x_3 axis.

then a Fourier series can be used to check that J_n has the expected behavior (see [30, Sec. 8.2]; [31, eq. (14)]; [32, Sec. 4]; and [20, eq. (7)]).

B. New Cone-Beam DCCs

We are only considering CB projections on a circular "source" trajectory, parametrized by $\lambda \in [0, 2\pi)$. The radius of the circle is R, and the unit vector $\alpha_\lambda = (\cos\lambda, \sin\lambda, 0)$ indicates the angular position in the $x_3 = 0$ plane. The CB projection of a 3-D function f is defined by

$$g_\lambda(\gamma) = \int_0^\infty f(R\alpha_\lambda + t\gamma)\, dt \tag{4}$$

where γ indicates the ray direction (so γ is an element of the unit sphere S^2). If a detector is now introduced, in the standard orientation and positioned at distance D from the source, we use unit vectors $\beta_\lambda = (-\sin\lambda, \cos\lambda, 0)$ and $e_3 = (0, 0, 1)$ to indicate the u and v directions, respectively, on the detector. See Fig. 1. The ray direction now becomes $\gamma_{u,v} = (u\beta_\lambda + ve_3 - D\alpha_\lambda)/\delta$ with $\delta = \sqrt{u^2 + v^2 + D^2}$. Recognizing D/δ as the cosine of the incidence angle on the detector, we define the usual cosine-weighted CB projection (see, for example, [33]–[36]) as

$$\hat{g}_\lambda(u, v) = \frac{D}{\delta} \int_0^\infty f(R\alpha_\lambda + t\gamma_{u,v})\, dt. \tag{5}$$

We now define

$$\hat{M}_n(\lambda) = \int_{-\infty}^\infty \int_{-\infty}^\infty \hat{g}_\lambda(u, v) \frac{u^n}{v^{n+2}}\, du\, dv. \tag{6}$$

Our main result is that if $\hat{g}_\lambda$ satisfies (5) for some function f, then for any nonnegative integer n, $\hat{M}_n(\lambda)$ is a homogeneous polynomial of degree n in $\cos\lambda$ and $\sin\lambda$:

$$\hat{M}_n(\lambda) = \sum_{k=0}^n a_k\ \cos^{n-k}\lambda\ \sin^k\lambda \tag{7}$$

(The case $n = 0$ has been presented in 2016 [29].) The $1/v^{n+2}$ term in the integral needs to be addressed. This singularity can be completely avoided if the compact support of f does not intersect the $x_3 = 0$ plane. For, in this case, we are ensured that for some $\varepsilon > 0$ we have $\hat{g}_\lambda(u, v) = 0$ for $|v| < \varepsilon$.

This mathematical requirement is too restrictive, because the common situation in practice is that the object being imaged is positioned near the center of the circle and would certainly intersect the source trajectory plane. Rather than avoiding the singularity, we will allow the support of f to intersect the $x_3 = 0$ plane, and we will handle the situation of $\hat{g}_\lambda(u, v) \neq 0$ for $v = 0$ as follows. We assume that f and $\hat{g}_\lambda$ are smooth functions and we replace $1/v^{n+2}$ by the distribution (generalized function) h_n which we define as an inverse Fourier transform:

$$h_n(s) = \int_{-\infty}^\infty H_n(\sigma)\, e^{2\pi i\sigma s}\, d\sigma \tag{8}$$

with

$$H_n(\sigma) = \frac{(-2\pi i)^{n+2}}{2(n+1)!}\, |\sigma|\, \sigma^n. \tag{9}$$

It is easily verified from (8) and (9) that for any nonzero scalar τ, we have $h_n(\tau s) = h_n(s)/\tau^{n+2}$ and therefore h_n is homogeneous of degree $-(n+2)$.

C. Demonstration of the New DCCs

We demonstrate (6) and (7) by a slightly circuitous route, via the following proposition. Let

$$M_n(\lambda) = \iint_{S^2} g_\lambda(\gamma)\, h_n(\gamma \cdot e_3)\, (\gamma \cdot \beta_\lambda)^n\, d\gamma. \tag{10}$$

We will show below that the right-hand sides of (10) and (6) are equal, so $M_n(\lambda) = \hat{M}_n(\lambda)$. The immediate goal, however, is to demonstrate that $M_n(\lambda)$ is a homogeneous polynomial of degree n in $\cos\lambda$ and $\sin\lambda$. To that end, we replace $g_\lambda(\gamma)$ with its definition (4), and apply the formula $h_n(\gamma) = t^{n+2} h_n(t\gamma)$ to obtain

$$\begin{aligned}
M_n(\lambda) &= \iint_{S^2} \int_0^\infty f(R\alpha_\lambda + t\gamma)\, dt\, h_n(\gamma \cdot e_3)\, (\gamma \cdot \beta_\lambda)^n\, d\gamma \\
&= \iint_{S^2} \int_0^\infty f(R\alpha_\lambda + t\gamma) h_n(t\gamma \cdot e_3)(t\gamma \cdot \beta_\lambda)^n t^2\, dt\, d\gamma \\
&= \iiint_{R^3} f(R\alpha_\lambda + x')\, h_n(x' \cdot e_3)\, (x' \cdot \beta_\lambda)^n\, dx' \\
&= \iiint_{R^3} f(x) h_n((x - R\alpha_\lambda) \cdot e_3)((x - R\alpha_\lambda) \cdot \beta_\lambda)^n\, dx \\
&= \iiint_{R^3} f(x)\, h_n(x \cdot e_3)\, (x \cdot \beta_\lambda)^n\, dx \\
&= \iiint_{R^3} f(x)\, h_n(x_3)\, (-x_1 \sin\lambda + x_2 \cos\lambda)^n\, dx
\end{aligned} \tag{11}$$

where we have performed the successive substitutions of variables $x' = t\gamma$ and $x = x' - R\alpha_\lambda$, and noting from their definitions that $\{\alpha_\lambda, \beta_\lambda, e_3\}$ form an orthonormal system. Finally,

TABLE I

VALUES OF $h_n^{(1/2\Delta)}(k\Delta)$, FROM (17)

n	$k=0$	k even	k odd
0	$\frac{-\pi^2}{2\Delta^2}$	0	$\frac{2}{k^2\Delta^2}$
1	0	$\frac{-k^2\pi^2}{2k^3\Delta^3}$	$\frac{-4+k^2\pi^2}{2k^3\Delta^3}$
2	$\frac{\pi^4}{24\Delta^4}$	$\frac{k^2\pi^2}{2k^4\Delta^4}$	$\frac{4-k^2\pi^2}{2k^4\Delta^4}$
3	0	$\frac{k^4\pi^4-12k^2\pi^2}{24k^5\Delta^5}$	$\frac{-k^4\pi^4+12k^2\pi^2-48}{24k^5\Delta^5}$
4	$\frac{-\pi^6}{720\Delta^6}$	$\frac{-k^4\pi^4+12k^2\pi^2}{24k^6\Delta^6}$	$\frac{k^4\pi^4-12k^2\pi^2+48}{24k^6\Delta^6}$

from (11) we immediately obtain

$$M_n(\lambda)=\sum_{k=0}^{n} a_k\ \cos^{n-k}\lambda\ \sin^k\lambda \tag{12}$$

with

$$a_k=\binom{n}{k}\iiint_{R^3} f(x)\,h_n(x_3)\,(-x_1)^k\,(x_2)^{n-k}\,dx. \tag{13}$$

Note that the above demonstration works equally well if $h_n(v)$ is replaced by the ordinary function $1/v^{n+2}$ (assuming the support of f is known to not intersect the plane $x_3=0$). Conversely, for the situation without this restriction, we replace $1/v^{n+2}$ by $h_n(v)$ in (6).

We now show that $M_n=\hat{M}_n$ which then establishes (7) via (12). From (10), the definition of M_n, we perform the change of variables $\gamma\to(u,v)$ using $\gamma=\gamma_{u,v}=(u\beta_\lambda+ve_3-D\alpha_\lambda)/\delta$ with $\delta=\sqrt{u^2+v^2+D^2}$. The Jacobian of this change of variables is $d\gamma=(D/\delta^3)\,du\,dv$, which can either be seen from a physicist's approach as the surface area subtended by a small rectangle $(du\,dv)$ at a distance δ which invokes a cosine-over-distance-squared formula of $(D/\delta)/\delta^2$, or can be seen by expressing $\gamma=(\gamma_1,\gamma_2,\gamma_3)$ in terms of standard polar coordinates, $\gamma=(\cos\phi\cos\theta,\sin\phi\cos\theta,\sin\theta)$, and by an explicit calculation of the partial derivatives $(d\phi\,/\,du$, etc.) to achieve $d\gamma=\cos\theta\,d\phi\,d\theta=(D/\delta^3)\,du\,dv$. Thus, starting from (10), and noting that the change of variables results in $\gamma\cdot e_3=v/\delta$ and $\gamma\cdot\beta_\lambda=u/\delta$,

$$\begin{aligned}
M_n(\lambda)&=\iint_{S^2} g_\lambda(\gamma)\,h_n(\gamma\cdot e_3)\,(\gamma\cdot\beta_\lambda)^n\,d\gamma\\
&=\iint_{R^2} g_\lambda(\gamma_{u,v})\,h_n(v/\delta)\,(u/\delta)^n\,(D/\delta^3)\,du\,dv\\
&=\iint_{R^2} g_\lambda(\gamma_{u,v})\,\delta^{n+2}h_n(v)\,(u/\delta)^n\,(D/\delta^3)\,du\,dv\\
&=\iint_{R^2} g_\lambda(\gamma_{u,v})\,h_n(v)\,u^n\,(D/\delta)\,du\,dv\\
&=\iint_{R^2} \hat{g}_\lambda(u,v)\,h_n(v)\,u^n\,du\,dv=\hat{M}_n(\lambda)
\end{aligned} \tag{14}$$

where we have associated $h_n(v)$ with $1/v^{n+2}$.

D. Implementing the Singularity at $v=0$

Starting with the Fourier transform pair for the Hilbert transform, we have

$$\frac{1}{\pi s}=\int(-i\,\mathrm{sgn}\,\sigma)\,e^{2\pi i\sigma s}\,d\sigma \tag{15}$$

valid outside a neighborhood of $s=0$. Taking successive derivatives and slightly simplifying this equation yields, on the right-hand side, the inverse Fourier transform of $H_n(\sigma)$ for $n=0,1,2\ldots$ [see (9)],

$$\begin{aligned}
\frac{1}{s^2}&=(-2\pi^2)\int|\sigma|\,e^{2\pi i\sigma s}\,d\sigma && (n=0)\\
\frac{1}{s^3}&=(2\pi^3 i)\int\sigma\,|\sigma|\,e^{2\pi i\sigma s}\,d\sigma && (n=1)\\
\frac{1}{s^4}&=\left(\frac{4\pi^4}{3}\right)\int\sigma^2\,|\sigma|\,e^{2\pi i\sigma s}\,d\sigma && (n=2)
\end{aligned} \tag{16}$$

and so on. We note that the $n=0$ case corresponds to the well-known "ramp-filter" of filtered backprojection image reconstruction. For numerical implementation of (6), we follow the textbook approach [37], [38] of band limiting the Fourier transform, setting the bandlimit B to $1/(2\Delta)$ where the sample spacing is Δ, and evaluating the result at $s=k\Delta$:

$$h_n^{(B)}(s)=\int_{-B}^{B} H_n(\sigma)\,e^{2\pi i\sigma s}\,d\sigma. \tag{17}$$

This procedure yields, for $n=0$ (see also [39]),

$$h_0^{(1/2\Delta)}(k\Delta)=\begin{cases}\dfrac{-\pi^2}{2\Delta^2} & k=0,\\ 0 & k\text{ even},\\ \dfrac{2}{k^2\Delta^2} & k\text{ odd}.\end{cases} \tag{18}$$

Table I gives the weights for $n=0\ldots4$. However, the singularities increase in severity with increasing n, so we propose using a more heavily regularized version:

$$\hat{h}_n^{(B)}(s)=\int_{B} H_n(\sigma)\,(1-|\sigma|/B)^{n+1}\,e^{2\pi i\sigma s}\,ds. \tag{19}$$

Table II lists the values of $\hat{h}_n^{(1/2\Delta)}(k\Delta)$ for $n=0\ldots4$.

TABLE II

VALUES OF $\hat{h}_n^{(1/2\Delta)}(k\Delta)$, FROM (19)

n	$k=0$	k even	k odd
0	$\frac{-\pi^2}{6\Delta^2}$	$\frac{2}{k^2\Delta^2}$	0
1	0	0	$\frac{-2}{k^3\Delta^3}+\frac{24}{\pi^2k^5\Delta^3}$
2	$\frac{\pi^4}{840\Delta^4}$	$\frac{2}{k^4\Delta^4}-\frac{120}{\pi^2k^6\Delta^4}$	0
3	0	0	$\frac{-2}{k^5\Delta^5}+\frac{360}{\pi^2k^7\Delta^5}-\frac{3360}{\pi^4k^9\Delta^5}$
4	$\frac{-\pi^6}{332640\Delta^6}$	$\frac{2}{k^6\Delta^6}-\frac{840}{\pi^2k^8\Delta^6}+\frac{30240}{\pi^4k^{10}\Delta^6}$	0

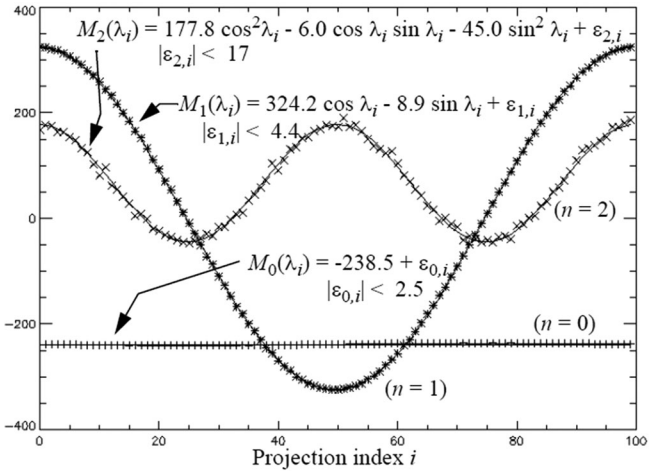

Fig. 2. Plots of $M_n(\lambda_i)$ [see (14)] for all 100 projections of the simplified and offset 3-D Shepp–Logan phantom, for $n=0,1,2$ (+, *, x, respectively). Fits of the nearest homogeneous polynomial of corresponding degree are shown with solid lines. The maximum deviation $\varepsilon_{n,i}$ is observed to be smaller for smaller n.

III. NUMERICAL EXAMPLES

The formulas of Table II were verified for $n=0,1,2$ using computer simulations of a half-size, simplified 3-D Shepp–Logan phantom (only the five large ellipsoids, numbered 1 through 5 in Table 1 of [40], were included), centered at $x=(3,0,3)$ so the phantom was offset but still intersected the trajectory plane $x_3=0$. All units are given in centimeters. The detector size was 51.4×51.4. The radius R was 50 and the detector distance D was 100. One hundred projections of size 1025×1025 detector pixels were simulated using analytic line-length calculations through the ellipsoids. The 100 source positions were uniformly spaced over the circle.

For each of the $i=1\ldots100$ projections, $M_n(\lambda_i)$ was computed using (6) with a simple trapezoid rule applied for the integral over u, and using the regularized $h_n(v)$ from Table II for the v integration. A three-point smoothing (with mask $[1,2,1]/4$) was applied in v five times successively and the Table II values were subsequently applied with Δ set to eight times the detector pixel spacing. Only cases $n=0,1,2$ are shown here.

Fig. 2 shows plots of the three curves $M_n(\lambda_i)$ for each of $n=0,1,2$. These curves were fitted to the nearest trigonometric polynomial, according to (7), with strong agreement, as illustrated in Fig. 2.

These numerical demonstrations were repeated after adding 1% and 5% Gaussian noise to the simulated projections. The resulting maximum derivations from the polynomials of Fig. 2 changed the bounds on $|\varepsilon_{n,i}|$ from 2.5, 4.4, 17 (noiseless, Fig. 2) to 4.0, 11.5, 23 (1% noise) and 13.2, 54.8, 100 (5% noise). These results suggest reasonably stable DCCs with respect to zero-mean noise.

IV. DISCUSSION AND CONCLUSION

For the limiting case of an infinite radius circular trajectory, the CB projections become 3-D parallel projections, which can be treated as independent 2-D problems in each plane parallel to $x_3=0$. Combining the Helgason–Ludwig conditions, (2), (3), in these planes immediately yields the CB DCCs, (6), (7).

For the case $n=0$, (10), (12), and (13) are related to [41, eq. (2.2)], [41, eq. (3.9)], and the equation prior to [41, eq. (3.5)] of [41], albeit in a different context.

Note: Both sides of (14) can be equivalently written as

$$M_n(\lambda)=\frac{1}{(n+1)!}\lim_{\varepsilon\to0}\int_{|v|>\varepsilon}\frac{q_\lambda^{(n+1)}(v)}{v}\,dv \tag{20}$$

where

$$q_\lambda^{(n+1)}(v)=\frac{d^{n+1}}{dv^{n+1}}\int_R\hat{g}_\lambda(u,v)\,u^n\,du \tag{21}$$

so $M_n(\lambda)$ is a principal value integral, and the increasing instability with n is manifest as nth-order derivatives.

The Helgason–Ludwig DCCs of (2) and (3) are necessary and sufficient. The new CB DCCs presented here are necessary conditions; we make no claim that they are also sufficient.

REFERENCES

[1] S. Helgason, *The Radon Transform.* Boston, MA, USA: Birkhauser, 1980.

[2] D. Ludwig, "The Radon transform on Euclidean space," *Commun. Pure Appl. Math.*, vol. 19, pp. 49–81, 1966.

[3] V. Aguilar, L. Ehrenpreis, and P. Kuchment, "Range conditions for the exponential Radon transform," *J. Anal. Math.*, vol. 68, pp. 1–13, 1996.

[4] F. Natterer, "Computerized tomography with unknown sources," *SIAM J. Appl. Math.*, vol. 43, pp. 1201–1212, 1983.

[5] F. Natterer and H. Herzog, "Attenuation correction in positron emission tomography," *Math. Methods Appl. Sci.*, vol. 15, pp. 321–330, 1992.

[6] A. Welch *et al.*, "Attenuation correction in PET using consistency information," *IEEE Trans. Nucl. Sci.*, vol. 45, no. 6, pp. 3134–3141, Dec. 1998.

[7] A. Bromiley *et al.*, "Attenuation correction in PET using consistency conditions and a three-dimensional template," *IEEE Trans. Nucl. Sci.*, vol. 48, no. 4, pp. 1371–1377, Aug. 2001.

[8] A. Welch, W. Hallett, P. Marsden, and A. Bromiley, "Accurate attenuation correction in PET using short transmission scans and consistency information," *IEEE Trans. Nucl. Sci.*, vol. 50, no. 3, pp. 427–432, Jun. 2003.

[9] A. Alessio, P. Kinahan, and K. Champley, "Attenuation-emission alignment in cardiact PET/CT based on consistency conditions," *Med. Phys.*, vol. 37, pp. 1191–1200, 2010.

[10] F. Natterer, "Determination of tissue attenuation in emission tomography of optically dense media," *Inverse Problems*, vol. 9, pp. 731–736, 1993.

[11] A. Welch, R. Clack, F. Natterer, and G. T. Gullberg, "Towards accurate attenuation correction in SPECT without transmission measurements," *IEEE Trans. Med. Imag.*, vol. 16, no. 5, pp. 532–541, Oct. 1997.

[12] I. Laurette, R. Clackdoyle, A. Welch, F. Natterer, and G. T. Gullberg, "Comparison of three applications of ConTraSPECT," *IEEE Trans. Nuc. Sci.*, vol. 46, no. 6, pp. 2146–2153, Dec. 1999.

[13] C. Mennessier, F. Noo, R. Clackdoyle, G. Bal, and L. Desbat, "Attenuation correction in SPECT using consistency conditions for the exponential ray transform," *Phys. Med. Biol.*, vol. 44, pp. 2483–2510, 1999.

[14] D. V. Finch and D. C. Solmon, "Sums of homogeneous function and the range of the divergent beam X-ray transform," *Numer. Funct. Anal. Optimization*, vol. 5, pp. 363–419, 1983.

[15] D. V. Finch and D. C. Solmon, "A characterization of the range of the divergent beam X-ray transform," *SIAM J. Math. Anal.*, vol. 14, pp. 767–771, 1983.

[16] S. K. Patch, "Moment conditions indirectly improve image quality," *Contemporary Mathematics*, vol. 278. Providence, RI, USA: AMS, 2001, pp. 193–205.

[17] G.-H. Chen and S. Leng, "A new data consistency condition for fan-beam projection data," *Med. Phys.*, vol. 32, pp. 961–967, 2005.

[18] Y. Wei, H. Yu, and G. Wang, "Integral invariants for computed tomography," *IEEE Signal Process. Let.*, vol. 13, no. 9, pp. 549–552, Sep. 2006.

[19] H. Yu, Y. Wei, J. Hsieh, and G. Wang, "Data consistency based translational motion artifact reduction in fan-beam CT," *IEEE Trans. Med. Imag.*, vol. 25, no. 6, pp. 792–803, Jun. 2006.

[20] R. Clackdoyle, "Necessary and sufficient consistency conditions for fan-beam projections along a line," *IEEE Trans. Nucl. Sci.*, vol. 60, no. 3, pp. 1560–1569, Jun. 2013.

[21] R. Clackdoyle, M. Defrise, L. Desbat, and J. Nuyts, "Consistency of fan-beam projections along an arc of a circle," in *Proc. 13th Int. Meeting Fully Three-Dimensional Image Reconstruction Radiol. Nucl. Med.*, Newport, RI, USA, May 31–Jun. 4, 2015, pp. 253–256.

[22] R. Clackdoyle and L. Desbat, "Data consistency conditions for truncated fan-beam and parallel projections," *Med. Phys.*, vol. 42, pp. 831–845, 2015.

[23] H. Yu, G. Wang, J. Yang, J. Pack, M. Jiang, and B. De Man, "Data consistency condition for truncated projections in fan-beam geometry," *J. X-ray Sci. Technol.*, vol. 23, pp. 627–638, 2015.

[24] F. John, "The ultrahyperbolic differential equation with four independent variables," *Duke Math. J.*, vol. 4, pp. 300–322, 1938.

[25] S. Patch, "Consistency conditions upon 3D CT data and the wave equation," *Phys. Med. Biol.*, vol. 47, pp. 2637–2650, 2002.

[26] M. S. Levine, E. Y. Sidky, and X. Pan, "Consistency conditions for cone-beam CT data acquired with a straight-line source trajectory," *Tsinghua Sci. Technol.*, vol. 15, pp. 56–61, 2010.

[27] R.Clackdoyle and L. Desbat, "Full data consistency conditions for cone-beam projections with sources on a plane," *Phys. Med. Biol.*, vol. 58, pp. 8437–8456, 2013.

[28] A. Aichert *et al.*, "Epipolar consistency in transmission imaging," *IEEE Trans. Med. Imag.*, vol. 34, no. 11, pp. 2205–2219, Nov. 2015.

[29] J. Lesaint, R. Clackdoyle, S. Rit, and L. Desbat, "Two cone-beam consistency conditions for a circular trajectory," in *Proc. 4th Int. Conf. Image Formation X-Ray Comput. Tomography*, 2016, pp. 431–434.

[30] S. Deans, *The Radon Transform and Some of Its Applications*. New York, NY, USA: Wiley, 1983.

[31] J. Prince and A. Willsky, "Constrained sinogram restoration for limited-angle tomography," *Opt. Eng.*, vol. 29, pp. 535–544, 1990.

[32] E. Clarkson and H. Barrett, "Symmetry properties of an imaging system and consistency conditions in image space," *Phys. Med. Biol.*, vol. 43, pp. 1039–1048, 1998.

[33] L. Feldkamp, L. Davis, and J. Kress, "Practical cone-beam algorithm," *J. Opt. Soc. Amer. A*, vol. 1, pp. 612–619, 1984.

[34] P. Grangeat, "Mathematical framework of cone-beam 3D reconstruction via the first derivative of the Radon transform," in *Proc. Math. Methods Tomography*, 1991, pp. 66–97.

[35] M. Defrise and R. Clack, "A cone-beam reconstruction algorithm using shift-variant filtering and cone-beam backprojection," *IEEE Trans. Med. Imag*, vol. 13, no. 1, pp. 186–195, Mar. 1994.

[36] H. Kudo and T. Saito, "Derivation and implementation of a cone-beam reconstruction algorithm for non-planar orbits," *IEEE Trans. Med. Imag.*, vol. 13, no. 1, pp. 196–211, Mar 1994.

[37] F. Natterer, *The Mathematics of Computerized Tomography.* New York, NY, USA: Wiley, 1986.

[38] A. C. Kak and M. Slaney, *Principles of Computerized Tomography Imaging.* New York, NY, USA: IEEE Press, 1988.

[39] G. Ramachandran and A. Lakshminarayanan, "Three-dimensional reconstruction from radiographs and electron micrographs: Application of convolutions instead of Fourier transforms," *Proc. Nat. Acad. Sci. USA*, vol. 68, pp. 2236–2240, 1971.

[40] M. Defrise and R. Clack, "Filtered backprojection reconstruction of combined parallel beam and cone beam SPECT data," *Phys. Med. Biol.*, vol. 40, pp. 1517–1537, 1995.

[41] B. Smith, "Image reconstruction from cone-beam projections: Necessary and sufficient conditions and reconstruction methods," *IEEE Trans. Med. Imag.*, vol. MI-4, no. 1, pp. 14–25, Mar. 1985.